Contribution from the Department of Chemistry,
The University of Michigan, Ann Arbor, Michigan 48109-1055

Structural Characterization of Paramagnetic, Triangulo Niobium Clusters, $Cp'_3Nb_3Cl_3(\mu_2\text{-}Cl)_3(\mu_3\text{-}O)(\mu_3\text{-}X)$ (X = OH, Cl)

M. David Curtis* and Julio Real

Received March 25, 1988

The Nb(III) complex $[Cp'Nb(CO)_2Cl_2]_2$ (**1**, Cp′ = C_5H_4Me) undergoes decarbonylation in refluxing THF to give a dark brown paramagnetic compound believed to be $Cp'_3Nb_3Cl_6(\mu_3\text{-}O)$ (**2**). Compound **2** reacts with atmospheric oxygen to produce $Cp'_3Nb_3Cl_3(\mu_2\text{-}Cl)_3(\mu_3\text{-}O)(\mu_3\text{-}OH)$ (**3**) and with chlorinated hydrocarbons to form $Cp'_3Nb_3Cl_3(\mu_2\text{-}Cl)_3(\mu_3\text{-}O)(\mu_3\text{-}Cl)$ (**4**). Compounds **3** and **4** are paramagnetic and exhibit 10-line ESR spectra characteristic of spin-$^1/_2$ systems with the odd electron coupled to only one Nb nucleus (g = 1.98, A = 158 G for **3**; g = 1.996, A = 155 G for **4**). X-ray structure determinations show that each of these clusters has one short Nb–Nb distance of ca. 2.92 Å corresponding to a Nb–Nb bond and two long Nb···Nb distances near 3.28 (**3**) or 3.39 Å (**4**). The Nb_3 triangle is bridged by Cl atoms along each edge and is capped by a μ_3-oxo ligand and a μ_3-hydroxo (**3**) or μ_3-chloro ligand (**4**) on opposite sides of the Nb_3 plane. Terminal Cp and Cl ligands complete the coordination sphere about each Nb atom. Crystal data: for **3**, a = 7.210 (2) Å, b = 26.097 (7) Å, c = 12.518 (3) Å, β = 94.18 (2)°, space group $P2_1/n$, Z = 4, V = 2349 Å^3, ρ_{calcd} = 2.06 g/mL, R = 0.039 and R_w = 0.054 on 2551 reflections with $I > 3\sigma(I)$; for **4**, a = 7.620 (1) Å, b = 15.108 (4) Å, c = 21.670 (6) Å, α = 87.45 (2)°, β = 93.68 (2)°, γ = 104.01 (2)°, space group $P\bar{1}$, Z = 4, V = 2414 (1) Å^3, ρ_{calcd} = 2.01 g/mL, R = 0.065 and R_w = 0.055 on 2424 reflections with $I > 3\sigma(I)$.

Introduction

As part of our continuing investigation[1] of metal–metal-bonded complexes of the early transition elements, we determined the structure of the Nb(III) dimer $[Cp'NbCl_2(CO)_2]$ (**1**, Cp′ = C_5H_4Me) prepared by Al reduction of $Cp'NbCl_4$ under 1 atm of CO as shown in eq 1.[2]

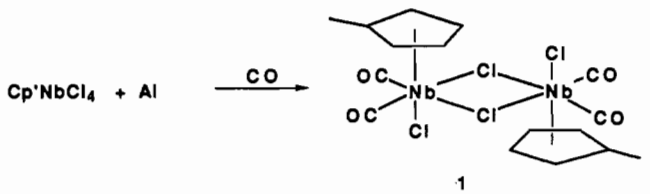

1 (1)

The reaction represented in eq 1 was reported originally to give the 18e monomer $CpNb(CO)_3Cl_2$.[3] We therefore wondered if an originally formed monomer had lost CO and dimerized through chloro-bridge bonds during the slow crystallization required for X-ray-quality crystals. To test this hypothesis, a THF solution of **1** was exposed to an atmosphere of CO at room temperature. IR spectra of this solution indicated no reaction. When the solution was heated under CO, it was found that complex **1** was decarbonylated. This paper reports the structures of two paramagnetic, triangulo clusters obtained from this reaction mixture upon subsequent oxidation by air or by halogenated hydrocarbons.

Experimental Section

All solvents were deaerated, dried (solvent/drying agent: CH_2Cl_2/P_2O_5; THF/CaH_2 followed by Na–K–benzophenone; aromatics and ethers/Na–K–benzophenone), distilled from the drying agent under pure N_2, and transferred to the inert-atmosphere box under N_2. The inert-atmosphere box was connected to a Vacuum Atmospheres MO-40-1V purifier.

NMR spectra were recorded on Bruker WM-360 or AM-300 machines. ESR spectra were obtained on a Bruker ER-200 X-band spectrometer. Elemental analyses were performed by Schwarzkopf Microanalytical Laboratory.

"$(Cp'NbCl_2)_3O$" and $Cp'_3Nb_3Cl_6(\mu_3\text{-}O)(\mu_3\text{-}OH)$ (3). A 500-mL Schlenk flask was fitted with a reflux condenser and a N_2 inlet and charged with 4.0 g (6.07 mmol) of **1** and 200 mL of THF. The flask was heated while N_2 was bubbled slowly through the solution. (The reaction proceeds in the same manner if the N_2 is replaced by CO.) The ν_{CO} bands were monitored periodically by IR spectroscopy. The intensities of the CO bands decreased with time, and no new bands were observed. After 2 h of gentle refluxing, the CO bands were extinct and the solution had changed from cherry red to very dark brown. The solution was transferred to the inert-atmosphere box and filtered through a 2-cm layer of dried, degassed Celite. The filtrate was concentrated to a volume of ca. 60 mL to give 0.7 g of a dark brown, microcrystalline product (**2**) insoluble in all common solvents except THF and CH_2Cl_2.

Compound **2** is paramagnetic as judged by its ^1H NMR spectrum (NMR (δ; 360 MHz, CD_2Cl_2): 12.0 ($w_{1/2}$ = 170 Hz); 27.1 ($w_{1/2}$ = 290 Hz); 36.0 ($w_{1/2} \approx$ 500 Hz)) but is ESR-silent at ambient temperature. Anal. Calcd for $Cp'NbCl_2$ ($C_6H_7Cl_2Nb$) and $Cp'_3Nb_3Cl_6O$ ($C_{18}H_{21}Cl_6Nb_3O$) (found): C, 29.66, 29.03 (30.20); H, 2.90, 2.82 (3.39); Cl, 29.19, 28.57 (30.74). Although the analysis fits better for $Cp'NbCl_2$, it is believed the compound is $Cp'_3Nb_3Cl_6O$ (see below).

A solution of 0.3 g of **2** in 6 mL of CH_2Cl_2 was placed in a long glass tube (10-mm diameter) and layered with 5 mL of hexane, and the tube was then capped with a rubber septum and allowed to stand for 3 weeks. At the end of this time, a crop of dark brown crystals (**3**) had formed. ESR: g = 1.98, A = 158 G (10 lines). IR: ν_{OH} = 3335 cm^{-1} (br, Nujol mull). Anal. Calcd for $Cp'_3Nb_3Cl_6(O)(OH)$ (found): C, 28.38 (28.16); H, 2.91 (2.78); Cl, 27.92 (28.02).

In a separate experiment, a CH_2Cl_2 solution of **2** was allowed to evaporate slowly to dryness in the inert-atmosphere box. The resulting crystals exhibited the same ESR and IR spectra in solution as **3** and were shown by X-ray analysis to be the solvate **3**·CH_2Cl_2 (see below).

$Cp'_3Nb_3Cl_6(\mu_3\text{-}O)(\mu_3\text{-}Cl)$ (4). A solution of 0.3 g of **2** in 5 mL of CH_2Cl_2 was placed in a flame-dried glass tube and layered with 4 mL of hexane, and the tube was sealed. After 3 weeks, a crop of dark brown crystals had formed. These were collected and washed with hexane. ESR: g = 1.996, A_{Nb} = 155 G (10 lines). Anal. Calcd for $Cp'_3Nb_3Cl_7O$ ($C_{18}H_{21}Cl_7Nb_3O$) (found): C, 27.71 (27.53); H, 2.71 (2.46); Cl, 31.81 (31.94).

Table I. Crystallographic Data for $Cp'_3NbCl_6(\mu_3\text{-}O)(\mu_3\text{-}OH)$ (**3**) and $Cp'_3Nb_3Cl_6(\mu_3\text{-}O)(\mu_3\text{-}Cl)$ (**4**)

Compound 3	
chem formula: $C_{18}H_{22}Cl_6Nb_3O_2$	fw: 762
a = 7.210 (2) Å	space group: $P2_1/n$
b = 26.097 (7) Å	T = 21 °C
c = 12.518 (3) Å	λ = 0.71069 Å
β = 94.18 (2)°	ρ_{calcd} = 2.06 cm^{-3}
V = 2349 (1) Å^3	μ = 20.7 cm^{-1}
Z = 4	transmission coeff: 0.54–0.73
	$R(F_o)$ = 0.039
	$R_w(F_o)$ = 0.054
Compound 4	
chem formula: $C_{18}H_{21}Cl_7Nb_3O$	fw: 780.5
a = 7.620 (1) Å	space group: $P\bar{1}$
b = 15.108 (4) Å	T = 21 °C
c = 21.670 (6) Å	λ = 0.71069 Å
α = 87.45 (2)°	ρ_{calcd} = 2.01 g cm^{-3}
β = 93.68 (2)°	μ = 20.15 cm^{-1}
γ = 104.01 (2)°	transmission coeff: 0.41–0.95
V = 2414 (1) Å^3	$R(F_o)$ = 0.065
Z = 4	$R_w(F_o)$ = 0.055

(1) Review: Curtis, M. D. *Polyhedron* **1987**, *6*, 759.
(2) Curtis, M. D.; Real, J. *Organometallics* **1985**, *4*, 940.
(3) Cardoso, A. M.; Clark, R. J. H.; Moorhouse, S. *J. Organomet. Chem.* **1980**, *186*, 237.

0020-1669/88/1327-3176$01.50/0

Table II. Fractional Atomic Coordinates for $Cp'_3Nb_3Cl_6(\mu_3\text{-}O)(\mu_3\text{-}OH)$ (3)

atom	x	y	z
Nb1	0.83870 (10)	0.29215 (3)	0.29856 (6)
Nb2	0.73895 (9)	0.38083 (3)	0.47111 (5)
Nb3	0.83079 (10)	0.39380 (3)	0.22028 (6)
Cl1	0.74202 (29)	0.28497 (8)	0.49132 (16)
Cl2	1.12432 (30)	0.25112 (9)	0.37527 (17)
Cl3	0.40622 (29)	0.38485 (10)	0.48841 (19)
Cl4	0.73461 (31)	0.45995 (8)	0.35655 (17)
Cl5	1.05136 (29)	0.32608 (9)	0.16328 (17)
Cl6	1.11235 (31)	0.44642 (10)	0.22607 (20)
C11	0.7065 (u5)	0.2063 (3)	0.2942 (7)
C12	0.5603 (13)	0.2448 (4)	0.2633 (10)
C13	0.6107 (19)	0.2639 (4)	0.1637 (9)
C14	0.7648 (19)	0.2423 (5)	0.1372 (9)
C15	0.8232 (14)	0.2083 (4)	0.2110 (8)
C16	0.7211 (25)	0.1704 (5)	0.3831 (10)
C21	0.7225 (11)	0.4145 (4)	0.6629 (6)
C22	0.8205 (12)	0.3685 (3)	0.6628 (7)
C23	0.9831 (11)	0.3764 (4)	0.6037 (7)
C24	0.9758 (11)	0.4257 (4)	0.5664 (7)
C25	0.8153 (13)	0.4496 (3)	0.5981 (7)
C26	0.5577 (15)	0.4262 (4)	0.7228 (8)
C31	0.7242 (13)	0.4579 (4)	0.0865 (7)
C32	0.8013 (13)	0.4162 (4)	0.0336 (7)
c33	0.6902 (14)	0.3722 (4)	0.0469 (7)
C34	0.5426 (12)	0.3875 (4)	0.1075 (7)
C35	0.5628 (12)	0.4393 (4)	0.1316 (7)
C36	0.7825 (16)	0.5118 (4)	0.0889 (10)
O1	0.9734 ()	0.3615 (2)	0.3674 (4)
O2	0.6628 (7)	0.3540 (2)	0.3182 (4)

Conversion of 2 to 1. A suspension of 0.2 g of **2** in THF was stirred with excess Al powder under 1 atm of CO. The solid slowly dissolved to give a dark red solution from which **1**, identified by comparison of its IR and NMR spectra with those of authentic material, was isolated in ca. 60% yield. Stirring **2** under CO alone gave no reaction.

X-ray Structure Determinations. Crystals were sealed in glass capillaries and mounted on a Syntex $P2_1$ diffractometer. Lattice parameters were obtained by least-squares analysis of 15 reflections scattered in reciprocal space, obtained from the automatic centering routine. Standard reflections were measured after every 50 data points. Crystallographic statistics are collected in Table I. Data were corrected for absorption.[4]

The structure of **3**, determined on crystals grown from CH_2Cl_2/hexane, was solved with the direct-methods program MULTAN[4] and refined with the XRAY[4] package of programs. All non-hydrogen atoms were refined with anisotropic temperature factors. H atoms were included at fixed, calculated positions with $B_H = 1.2B_C$, where B_C is the isotropic temperature factor of the carbon to which the H atom is bonded.

Final atomic coordinates are listed in Table II and selected bond distances given in Table III. (More extensive tables of distances and angles are in the supplementary material.) Tables of temperature factors and F_o vs F_c are in the supplementary material.

A crystal of **3**, obtained from evaporating a CH_2Cl_2 solution of **2**, was also mounted. The crystal was found to be triclinic, space group $P\bar{1}$, with $a = 13.913$ (3) Å, $b = 16.084$ (3) Å, $c = 13.213$ (4) Å, $\alpha = 92.95$ (2)°, $\beta = 114.38$ (2)°, $\gamma = 92.79$ (2)°, $Z = 4$, $V = 2682$ (1) Å^3, and $\rho_{calcd} = 1.85$ g/mL. The structure was solved ($R_1 = 0.040$, $R_2 = 0.034$ on 7048 reflections with $I > 3\sigma(I)$), and the compound was shown to be $3{\cdot}CH_2Cl_2$, i.e. a solvate of **3**. At the molecular level, the structures of the triangulo clusters in the solvated and unsolvated crystals were identical within experimental error.

The structure of **4** was obtained from crystals obtained as described above. Table I lists relevant statistics. The intensity of the check reflections decayed approximately 38% during data collection, limiting data to $2\theta = 35°$. A linear decay correction was applied to the data, which were then corrected for absorption,[4] and the structure was solved with MULTAN. Refinement utilized the SHELX76[4] X-ray package. The Nb and Cl atoms were refined anisotropically, but the carbon atoms were refined with isotropic temperature factors due to the small number of reflections. Hydrogen atoms were not included in the refinement.

Final atomic positions are listed in Table IV, and selected bond distances are in Table III. (More extensive tables of distances and angles are in the supplementary material.) Temperature factors and a listing of F_o vs F_c are in the supplementary material.

(4) Two crystallographic program packages were used. The older "XRAY" package contained the programs SYNCOR (W. Schmonsees, data reduction), FORDAP (A. Zalkin, Fourier electron density synthesis), ORFLS (W. R. Busing, K. O. Martin, and H. A. Levy, least-squares refinement), ORFFE (W. R. Busing, K. O. Martin, and H. A. Levy, crystallographic function and error program for calculating bond distances and angles), HFINDR (A. Zalkin, calculated hydrogen atom positions), ABSORB (D. Templeton and L. Templeton, numerical absorption correction), and MULTAN-78 (P. Main, direct methods). The newer SHELX package (C. M. Sheldrick, package for crystal structure determination) includes routines for direct methods, Fourier synthesis, least-squares refinements, and numeric absorption correction. ORTEP-II (C. K. Johnson) was used to generate thermal ellipsoid plots. Scattering factors were taken from: *International Tables for X-ray Crystallography*; Ibers, J. A., Hamilton, W. C., Eds.; Kynoch: Birmingham, England, 1974; Vol. IV. In both packages, the function $\Sigma w(|F_o| - |F_c|)^2$ is minimized. The weighting scheme used by XRAY is $w = 4F_o^2/[\sigma^2(F_o^2) + p^2F_o^4]$, where $p = 0.04$. The weighting scheme used by SHELX is $w = 1/(\sigma^2(F_o) + pF_o^2)$, where $p = 0.0001$.

Table III. Selected Bond Distances for **3** and the Two Independent Molecules of **4**[a]

bond	3	4A	4B
Nb1–Nb3	2.827 (1)	2.921 (3)	2.934 (3)
Nb1···Nb2	3.281 (1)	3.405 (3)	3.392 (3)
Nb2···Nb3	3.274 (1)	3.377 (3)	3.379 (3)
Nb1-OH	2.200 (5)		
Nb3-OH	2.209 (5)		
Nb2-OH	2.263 (5)		
Nb1-O	2.079 (5)	2.033 (11)	2.047 (12)
Nb3-O	2.065 (5)	2.054 (11)	2.045 (11)
Nb2-O	2.074 (5)	2.044 (11)	2.051 (11)
Nb-Cl(t)[b]	2.423 [6]	2.44 [2]	2.44 [2]
Nb2-Cl1,4[b]	2.514 [3]	2.524 [5]	2.524 [9]
Nb1,3-Cl1,4[b]	2.562 [6]	2.59 [1]	2.58 [1]
Nb1,3-Cl5[b]	2.520 [8]	2.507 [7]	2.508 [8]
Nb2-Cl(μ_3)		2.786 (6)	2.781 (6)
Nb1,3-Cl(μ_3)		2.585 [8]	2.585 [8]
Nb-C(Cp')[b]	2.42 [6]	2.40 [8]	2.41 [5]

[a] Numbering scheme as in I (see text). [b] Average values. Numbers in brackets are the standard deviations of the average.

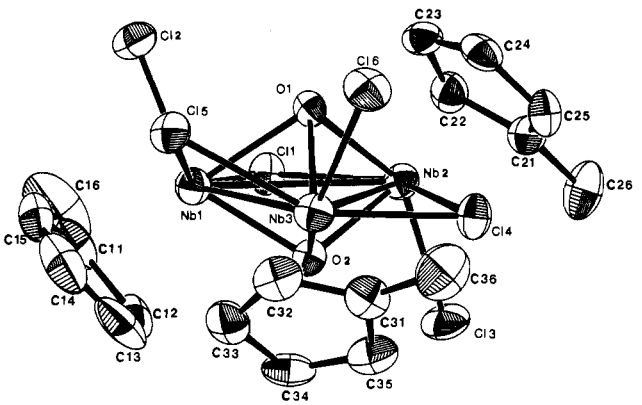

Figure 1. ORTEP drawing of $[Cp'NbCl_2]_3(\mu_3\text{-}O)(\mu_3\text{-}OH)$ (**3**). The numbering scheme corresponds to the atomic positions in Table II.

Results and Discussion

Gentle heating of THF solutions of $[Cp'NbCl_2(CO)_2]_2$ (**1**) results in its decarbonylation at CO pressures ≤1 atm. The product of this decarbonylation reaction, a black powder, is analyzed as $[Cp'NbCl_2]_n$. This powder does not react with CO but does react with Al powder under a CO atmosphere to regenerate **1**. Therefore, it appears that **1** is oxidized upon decarbonylation, and we tentatively formulate **2** as a μ_3-oxo trimer on the basis of these data and the subsequent reactions of **2** (see below). The source of the oxygen may be either the THF or the CO.

$$\underset{\mathbf{1}}{[Cp'NbCl_2(CO)]_2} \underset{\text{Al, +CO}}{\overset{\Delta,\ \text{THF, -CO}}{\rightleftharpoons}} \underset{\mathbf{2}}{[Cp'NbCl_2]_3O} \qquad (2)$$

Compound **2** is paramagnetic and exhibits three broad resonances in its ^{1}H NMR spectrum at δ 12.0, 27.1, and 36.0, which may correspond to the three types of hydrogen in the Cp′ ligand.

Table IV. Fractional Atomic Coordinates for $Cp'_3Nb_3Cl_6(\mu_3\text{-}O)(\mu_3\text{-}Cl)$ (**4**)[a]

atom	x	y	z	U_{iso}, Å^2	atom	x	y	z	U_{iso}, Å^2
Nb1	0.1028 (3)	−0.1831 (1)	0.0969 (1)	0.031	Nb4	0.3457 (3)	0.3757 (1)	0.3517 (1)	0.030
Nb2	−0.0176 (3)	−0.2402 (1)	0.2209 (1)	0.030	Nb5	0.1331 (3)	0.2156 (1)	0.2861 (1)	0.033
Nb3	−0.1079 (3)	−0.4060 (1)	0.1140 (1)	0.031	Nb6	0.2521 (3)	0.1769 (1)	0.4359 (1)	0.037
O1	−0.1112 (16)	−0.2743 (8)	0.1325 (5)	0.030	O2	0.3378 (16)	0.2389 (7)	0.3537 (5)	0.018
ClO1	0.2172 (7)	−0.3031 (3)	0.1661 (2)	0.034	Cl02	0.0299 (7)	0.2832 (3)	0.3814 (3)	0.039
Cl1	−0.1277 (8)	0.8486 (4)	0.0221 (o)	0.051	Cl4	0.6747 (8)	0.3964 (4)	0.3607 (3)	0.055
Cl2	0.6656 (8)	0.7529 (4)	0.2408 (3)	0.047	Cl5	0.3072 (9)	0.1183 (4)	0.2434 (o)	0.058
Cl3	1.0788 (8)	0.4847 (4)	0.1193 (3)	0.048	Cl6	0.0233 (9)	0.1586 (4)	0.5109 (3)	0.058
Cl13	0.0756 (8)	0.6794 (3)	0.0276 (3)	0.044	Cl45	0.3855 (8)	0.3375 (j)	0.2431 (3)	0.052
Cl23	0.8706 (7)	0.5836 (3)	0.2298 (2)	0.033	Cl46	0.3854 (8)	0.3390 (4)	0.4689 (2)	0.044
Cl12	−0.0434 (8)	0.9052 (3)	0.1652 (3)	0.044	Cl56	0.0296 (8)	0.0786 (3)	0.3613 (3)	0.042
C11	0.3111 (32	0.9071 (15)	0.0244 (11)	0.052	C41	0.2438 (29)	0.5011 (13)	0.3926 (10)	0.038
C12	0.2662 (30)	0.9669 (14)	0.0647 (10)	0.047	C42	0.4268 (29)	0.5331 (13)	0.3785 (10)	0.037
C13	0.3449 (30)	0.9497 (14)	0.1231 (10)	0.044	C43	0.4410 (29)	0.5324 (13)	0.3147 (9)	0.034
C14	0.4385 (32)	0.8764 (15)	0.1188 (10)	0.052	C44	0.2668 (31)	0.4993 (14)	0.2869 (10)	0.041
C15	0.4024 (32)	0.8485 (15)	0.0547 (11)	0.049	C45	0.1397 (29)	0.4784 (13)	0.3359 (9)	0.035
C16	0.2615 (38)	−0.0969 (17)	−0.0471 (12)	0.084	C46	0.1662 (33)	0.4994 (15)	0.4558 (11)	0.060
C21	0.0244 (30)	0.7423 (14)	0.3326 (10	0.046	C51	0.8327 (35)	0.1408 (17)	0.2385 (12)	0.068
C22	0.1887 (27)	0.7347 (13)	0.3044 (9)	0.030	C52	0.95555 (36)	0.1584 (17)	0.1901 (12)	0.073
C23	0.2612 (29)	0.8213 (14)	0.2761 (10)	0.041	C53	0.0224 (36)	0.2511 (17)	0.1856 (12)	0.076
C24	0.1550 (29)	0.8831 (13)	0.2878 (9)	0.036	C54	0.9372 (36)	0.2943 (16)	0.2313 (12)	0.068
C25	1.0063 (28)	0.8338 (13)	0.3225 (9)	0.034	C55	0.8200 (32)	0.2250 (16)	0.2628 (10)	0.058
C26	0.9050 (30)	0.6685 (14)	0.3716 (10)	0.050	C56	0.7206 (41)	0.0411 (19)	0.2545 (13)	0.100
C31	0.6564 (30)	0.4595 (14)	0.0864 (10)	0.048	C61	0.4791 (35)	0.1456 (16)	0.5108 (12)	0.062
C32	0.7152 (31)	0.5137 (15)	0.0318 (10)	0.052	C62	0.3376 (34)	0.0622 (15)	0.5063 (11)	0.057
C33	0.6666 (34)	0.5993 (16)	0.0389 (11)	0.064	C63	0.3203 (34)	0.0337 (16)	0.4451 (11)	0.061
C34	0.5841 (33)	0.5971 (16)	0.0966 (11)	0.062	C64	0.4550 (35)	0.0915 (16)	0.4129 (11)	0.067
C35	0.5771 (29)	0.5118 (14)	0.1243 (9)	0.043	C65	0.5582 (32)	0.1624 (15)	0.4523 (11)	0.057
C36	0.6546 (35)	0.3571 (16)	0.1005 (11)	0.072	C66	0.5402 (45)	0.1973 (21)	0.5680 (15)	0.125

[a] Numbering scheme:

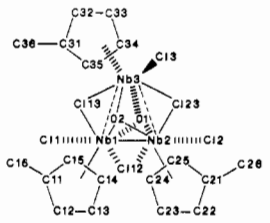

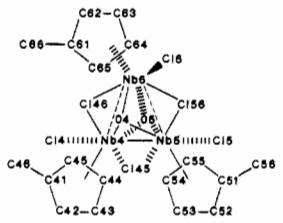

As expected, **2** is ESR-silent at ambient temperature.

An attempt to crystallize **2** led instead to a low yield of dark brown crystals (**3**), solutions of which exhibit an intense 10-line ESR pattern with A_{Nb} = 158 G centered at g = 1.98. Exposing a CH_2Cl_2 solution of **2** to air for a few seconds also causes an identical ESR signal to appear immediately. The crystalline **3** exhibits a ν_{OH} stretch at 3335 cm^{-1}, whereas **2** has no such absorption. An X-ray structure determination of **3** reveals its structure to be $[Cp'NbCl_2]_3(\mu_3\text{-}O)(\mu_3\text{-}OH)$.

The source of the hydrogen atom in the hydroxyl group is not known, but possibilities are surface hydroxyls on the glass, solvent, or traces of water. Another attempt to crystallize **2** from CH_2Cl_2 in a sealed, flame-dried tube resulted in a low yield of the new triangulo cluster $[CpNbCl_2]_3(\mu_3\text{-}O)(\mu_3\text{-}Cl)$ (**4**), the structure of which was determined by X-ray crystallography. Solutions of cluster **4** also exhibit an intense ESR signal with g = 1.996 and A_{Nb} = 155 G. Solid **2** reacts rapidly with chloroform to give **4**.

General Description of the Structures of 3 and 4. The molecular structures of $[Cp'NbCl_2]_3(\mu_3\text{-}O)(\mu_3\text{-}OH)$ (**3**) and $[Cp'NbCl_2]_3(\mu_3\text{-}O)(\mu_3\text{-}Cl)$ (**4**) are very similar. Both compounds consist of an isosceles triangle of three Nb atoms with one short Nb–Nb contact and two long ones (see Figures 1 and 2). Each edge of the triangle is bridged by one chlorine atom, and opposite faces of the triangle are triply bridged by a μ_3-oxo ligand and either a μ_3-OH (**3**) or a μ_3-Cl ligand (**4**). Terminal Cp and Cl ligands on each Nb complete the coordination sphere.

In both compounds the Cp groups attached to the two Nb atoms which are bonded together are mutually cis with respect to the Nb_3 plane while the third Cp group is trans to the other two with respect to this plane. The μ_2-Cl between the bonded Nb atoms is displaced out of the Nb_3 plane while the other two μ_2-Cl ligands lie in the Nb_3 plane. The displacement of the first μ_2-chloride is probably due to steric repulsion from the two cis-Cp groups.

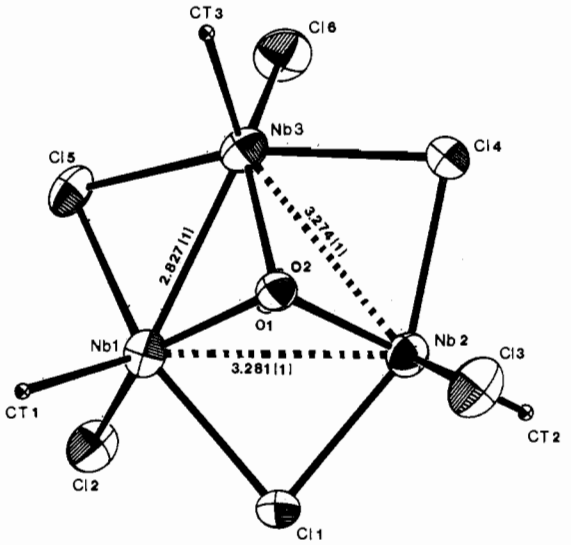

Figure 2. ORTEP view of the inner coordination sphere of **3** perpendicular to the plane of the Nb atoms.

Curiously, the placement of the μ_3-oxo ligand is on opposite sides of the Nb_3 plane in **3** and **4**. In **3**, the μ_3-oxo ligand lies on the same side of the plane as the two cis-Cp groups, whereas in **4** the μ-oxo ligand is on the other side.

A formal oxidation state of Nb(IV) can be assigned to each Nb atom, which leaves each Nb with a d^1 configuration. Two d electrons couple to form one Nb–Nb bond, leaving one unpaired electron on the non-metal–metal-bonded Nb. The ESR spectra of **3** and **4** are characteristic of an $S = {}^1/_2$ system coupled to one Nb ($I = {}^9/_2$) nucleus. These structural relationships are diag-

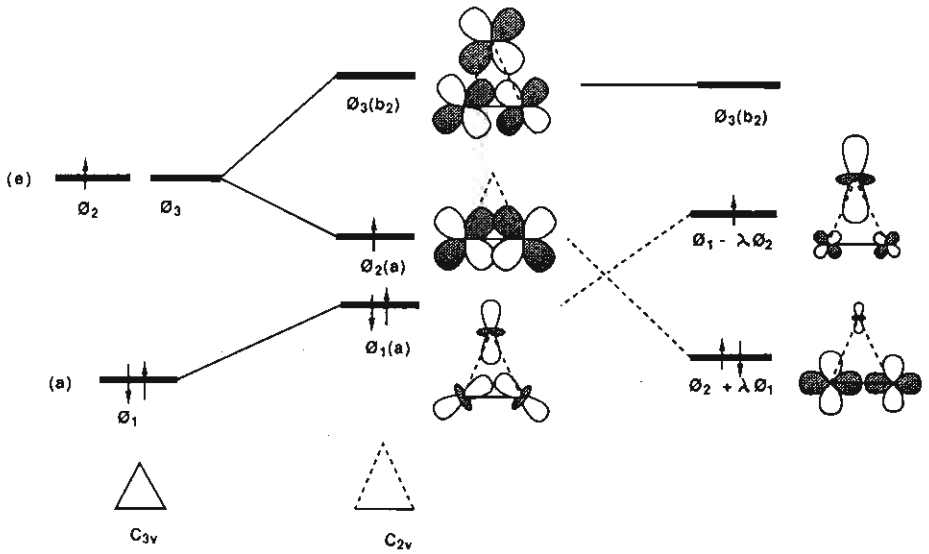

Figure 3. Schematic of the effects of a C_{2v} distortion and a forbidden crossover on the a + e orbitals of an equilateral triangulo cluster.

rammed in I, which shows the numbering scheme used in Table III.

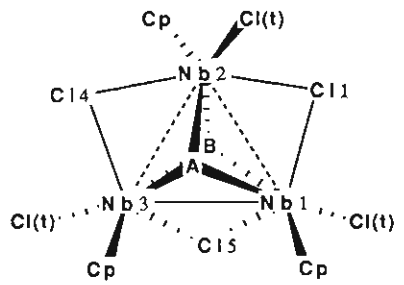

I

3: A =O, B= OH

4: A =Cl, B = O

Structural Details. Figure 1 is an ORTEP plot of **3**, which shows the numbering scheme used for the atomic positions reported in Table II. Figure 2 is a view of the inner core perpendicular to the Nb_3 plane. Selected bond distances are compiled in Table III. In some cases, average values are given when the individual distances were statistically identical. Table III also contains selected distances for the two independent molecules **4A** and **4B**. Again, average values are presented where appropriate. To facilitate comparisons, the numbering scheme shown in I is used in Table III.

Although the hydrogen atom of the μ_3-OH group was not located, the pattern of Nb–O distances leaves no doubt about the identity of the bridging hydroxyl group. The average Nb–O distance to one oxygen is 2.20 [1] Å and to the other is 2.07 [1] Å. The oxygen with the longer Nb–O distances is assigned to the μ_3-hydroxyl group.

The Nb1–Nb3 bond lengths in **3** and **4** are consistent with a Nb–Nb single bond. This bond is about 0.1 Å shorter in **3** than in **4**. The Nb···Nb nonbonded distances in **3** (average 3.277 [5] Å) are also ca. 0.1 Å shorter than the corresponding distances in **4** (average 3.388 [13] Å). The contraction of the Nb–Nb distances in **3** is undoubtedly a reflection of the smaller size of the μ_3-OH group as compared to that of the μ_3-Cl.

As expected, the Nb–Cl distances show the trend Nb–Cl(terminal) < Nb–Cl(μ_2) < Nb–Cl(μ_3), but within this trend some interesting variations occur. The μ_3-Cl ligand in **4** lies ca. 0.2 Å closer to the "bonded" Nb atoms at the base of the isosceles triangle than to the nonbonded Nb atom at the apex of the triangle (the μ_3-OH group in **3** also displays this feature). The opposite pattern is seen with the μ_2-chlorides (Cl(1) and Cl(4)): these lie closer to the nonbonded Nb atom at the apex. However, the Nb–Cl(5) distances that span the Nb–Nb bond are also relatively short. A contraction of M–X distances when X bridges a M–M bond has been noted previously and is apparently a general phenomenon.[5]

Bonding. Several theoretical treatments of triangulo clusters have appeared.[6] Clusters **3** and **4** present some interesting new facets to these discussions of bonding since, to our knowledge, these clusters have the fewest number (three) of electrons available for metal–metal bonding of any triangulo cluster yet reported and the hyperfine pattern establishes that the one electron is localized on only one Nb center.

Clusters **3** and **4** belong to the classification B_3 used in ref 6a. All calculations agree that the three metal–metal orbitals of lowest energy in regular (C_3 symmetry or higher) triangulo clusters of this classification have symmetry a + e (see Figure 3). If we neglect for the moment the fact that the cis, cis, trans arrangement of the terminal Cp and Cl ligands reduces the symmetry of **3** and **4** to C_{2v} (and thus removes any degeneracies), three electrons occupying an a + e set of orbitals would give rise to a ^2E state and would be susceptable to a Jahn–Teller distortion (both first *and* second order in this case). Reference 6a has discussed these distortions, and one possible distortion leads to a shortening of one M–M distance and a lengthening of the other two in the M_3 triangle. What effect would such a distortion have on a three-electron M_3 cluster?

As Figure 3 shows, this distortion would increase the antibonding character and decrease the bonding character of ϕ_3, and increase the bonding interactions in ϕ_2. As a result, the doubly degenerate level will split with the energy of ϕ_2 decreasing and the energy of ϕ_3 increasing. Following the distortion, the electron configuration would be $\phi_1^2\phi_2^1$.

However, as seen in Figure 3, ϕ_2 is delocalized over the two bonded metals, a result clearly in contradiction to the ESR results. Obviously another effect must come into play, and we propose this to be a rehybridization of ϕ_1 and ϕ_2 as a consequence of a forbidden crossing. The symmetries of the orbitals ϕ_2 and ϕ_3 after the distortion are a_1 and b_2, respectively. Orbitals ϕ_1 and ϕ_2 now have the same symmetry and will interact with the result shown in Figure 3. The lower energy orbital, $\phi_2 + \lambda\phi_1$, becomes more localized in the M–M bond, while the combination $\phi_1 - \lambda\phi_2$ becomes more localized on the unique, nonbonded metal. This orbital is singly occupied, so the spin density resides primarily on one metal in agreement with the ESR results.

Finally, we note that the μ_3 capping ligands are predicted to move *with* the nonbonded atom in $Mo_3(\mu_3\text{-}S)_2Cl_9^{3-}$ as a result of the Jahn–Teller distortion.[6a] In **3** and **4**, the μ_3-oxo ligand does appear to move with the nonbonded atom (all Nb–O bond lenghths

(5) Curtis, M. D.; Fotinos, N. A.; Han, K. R.; Butler, W. M. *J. Am. Chem. Soc.* **1983**, *105*, 2686.

(6) For leading references, see: (a) Jiang, Y.; Tang, A.; Hoffmann, R.; Huang, J.; Lu, J. *Organometallics* **1985**, *4*, 27. (b) Hofmann, P.; Rösch, N.; Schmidt, H. R. *Inorg. Chem.* **1986**, *25*, 4470. (c) Bursten, B. E.; Cotton, F. A.; Hail, M. B.; Najjar, R. C. *Ibid.* **1982**, *21*, 302.

are statistically equivalent) while the μ_3-OH and μ_3-Cl ligands either stay put or move toward the bonded pair of metals.

Acknowledgment. We thank the National Science Foundation (Grant No. CHE-83-05235) for support of this research. J.R. also thanks the Department of Chemistry for Riggs, Knoller, and Fenwich Fellowships and the U.S.-Spanish Joint Committee for Cultural and Educational Cooperation for a fellowship.

Supplementary Material Available: Tables V and VI (bond distances and angles for **3** and **4**) and Tables VII and VIII (temperature factors for **3** and **4**) (10 pages); Tables IX and X (F_o vs F_c for **3** and **4**) (20 pages). Ordering information is given on any current masthead page.

Contribution from the Eastern Regional Research Center, USDA—ARS, 600 East Mermaid Lane, Philadelphia, Pennsylvania 19118, and Department of Chemistry and Materials Science Center, Cornell University, Ithaca, New York 14853

Isomorphous Substitution in Phyllosilicates as an Electronegativity Perturbation: Its Effect on Bonding and Charge Distribution

William F. Bleam*,† and Roald Hoffmann‡

Received November 10, 1987

Isomorphous substitution in 2:1 phyllosilicates is typified by the substitution of Si(IV) by Al(III) in the tetrahedral sheet and Al(III) by Mg(II) in the octahedral sheet. Qualitative perturbation theory and extended Hückel, tight-binding calculations show that most of the excess negative charge not remaining at the substitution site is deposited on nearest-neighbor oxygens in the Al(III) → Si(IV) case. Nearest-neighbor oxygens are bypassed and most of the displaced negative charge appears on next-nearest-neighbor aluminum atoms in the Mg(II) → Al(III) case. Next-nearest-neighbor interactions dominate when there are negligible orbital interactions between the nearest-neighbor oxygen atoms and the substituting atom. The electronegativity perturbation in the cases we studied causes the bonds in the polyhedra where the substitution occurs to lengthen, bonds in adjacent polyhedra to shorten, and the atomic populations to increase on the nearest- and next-nearest neighbor atoms.

Introduction

The negative charge on a phyllosilicate mineral (e.g., mica or smectite) layer results from isomorphous substitution of structural cations of higher valence by others with lower valence, e.g. Al(III) replacing Si(IV) in the tetrahedral sheet (viz., $Al(III)_{tet} \rightarrow Si(IV)_{tet}$) or Mg(II) replacing Al(III) in the octahedral sheet (viz., $Mg(II)_{oct} \rightarrow Al(III)_{oct}$). The excess negative charge is locally balanced by cations located *between* the layers. This phenomena is quite common in phyllosilicates where the ratio of tetrahedral sheets to octahedral sheets is 2:1 (Figure 1) and is an important property used in their classification.[1-4]

Mineralogists and chemists have long speculated on the distribution of excess negative charge arising from isomorphous substitution in phyllosilicates. According to Radoslovich,[5] the apical oxygens in celadonite, a mica with layer-charge arising from octahedral substitution of Al(III) by Mg(II), carry the excess negative charge. Sposito[6] suggests isomorphous substitution of tetrahedral Si(IV) by Al(III) deposits excess negative charge principally on the basal oxygens of the "siloxane ditrigonal" cavity, enhancing the Lewis base character of the cavity.

We have shown[7] the electronic structure of neutral-layer phyllosilicates can be viewed as essentially tetrahedral silicate sheets (Figure 2) perturbed by interactions with octahedral cations. We will indicate primitive cell stoichiometry and the two-dimensional, infinite topology of the tetrahedral sheets with the symbol $^2_\infty[Si_2O_5^{2-}]$. Given this, we can greatly simplify our investigation of tetrahedral substitution by examining *isolated* aluminosilicate tetrahedral sheets, $^2_\infty[Al_xSi_{2-x}O_5^{(2+x)-}]$. Our model for "octahedral-sheet" substitution will be $Mg(II)_{oct} \rightarrow Al(III)_{oct}$ and will rely on comparisons of pyrophyllite ($^2_\infty[Al_2(OH)_2(Si_2O_5)_2]$) and celadonite ($K^+$, $^2_\infty[MgAl(OH)_2(Si_2O_5)_2^-]$).

All calculations were done with use of the extended Hückel, tight-binding method.[8-10] Considerable experience at the molecular level using extended Hückel theory allows us to distill a chemist's interpretation from the inherently delocalized nature of solid-state interactions. Details relevant to our calculations are found in the Appendix and Tables VI and VII.

Bonding in Phyllosilicates

A picture of the electronic structure of silicates has emerged from the numerous quantum-chemical[11,12] and solid-state theoretical studies[13-15] over the years. The electronic states fall into two *groups* of bands, the "O(2p)" bands and the "O(2s)" bands. The uppermost occupied states are nonbonding (viz., "lone-pair" electron) states derived from O(2p) orbitals. States derived from interactions between Si(3p) and O(2p) orbitals are found at energies directly below the nonbonded O(2p) states. The stronger Si(3s)–O(2p) interactions lead to the states found at the bottom of the O(2p) group of bands. The energy range from the top of the O(2p) group of bands to the bottom is about 10 eV.[14,16-20] The

† Eastern Research Center, USDA—ARS.
‡ Cornell University.

(1) Grim, R. E. *Clay Mineralogy*; McGraw-Hill: New York, 1968; p 34.
(2) van Olphen, H. *An Introduction to Clay Colloid Chemistry*; Wiley: New York, 1977; p 67.
(3) Brown, G.; Newmann, A. C. D.; Rayner, J. H.; Weir, A. H. In *The Chemistry of Soil Constituents*; Greenland, D. J., Hayes, M. H. B., Eds.; Wiley: New York, 1978; pp 29-178.
(4) Bailey, S. W. In *Crystal Structures of Clay Minerals and Their X-Ray Identification*; Brindley, G. W., Brown, G., Eds.; Mineralogical Society: London, 1980; pp 2-124.
(5) Radoslovich, E. W. *Am. Mineral.* **1963**, *48*, 76.
(6) Sposito, G. *The Surface Chemistry of Soils*; Oxford University Press: New York, 1984; p 15.
(7) Bleam, W.; Hoffmann, R. *Phys. Chem. Miner.*, in press.
(8) Hoffmann, R. *J. Chem. Phys.* **1963**, *39*, 1397.
(9) Hoffmann, R.; Lipscomb, W. N. *J. Chem. Phys.* **1962**, *36*, 2179.
(10) Whangbo, M.-H.; Hoffmann, R.; Woodward, R. B. *Proc. R. Soc. London, A* **1979**, *366*, 23.
(11) Tossell, J. A.; Gibbs, G. V. *Phys. Chem. Miner.* **1977**, *2*, 21.
(12) Gibbs, G. V. *Am. Mineral.* **1982**, *67*, 421.
(13) Griscom, D. L. *J. Non-Cryst. Solids* **1977**, *24*, 155.
(14) Pantelides, S. T. *Comments Solid State Phys.* **1977**, *8*, 55.
(15) Harrison, W. A. In *The Physics of SiO_2 and Its Interfaces*; Pantelides, S. T., Ed.; Pergamon: New York, 1978; pp 105-109.
(16) DiStefano, T. H.; Eastman, D. E. *Phys. Rev. Lett.* **1971**, *27*, 1560.
(17) Tossell, J. A.; Vaughan, D. J.; Johnson, K. H. *Chem. Phys. Lett.* **1973**, *20*, 329.
(18) Schneider, P. M.; Fowler, W. B. *Phys. Rev. Lett.* **1976**, *36*, 425.
(19) Schlüter, M.; Chelikowsky, J. R. *Solid State Comm.* **1977**, *21*, 381.

0020-1669/88/1327-3180$01.50/0